A perturbed ghost model for estimating air-gun array signatures

Rob Telling[1] and Sergio Grion[1]

https://doi.org/10.1190/tle38090692.1.

Abstract

Source designature for seismic data acquired using an air-gun array aims to remove the effects of pulse asymmetry, bubble oscillation, array directivity, and ghosting at the sea surface. For the process to be successful, we require an accurate representation of the source signature in the far field over the full data bandwidth. The well-established approach to this problem is to derive signatures from hydrophone data recorded in the near field of the source array. We perform a least-squares inversion of the near-field data, using a representation of the physics of propagation within the vicinity of the array, according to the measured geometry and incorporating bubble motion and source ghost formation. While ghost formation is typically treated using a simple linear model of propagation and reflection at the sea surface, observations suggest that this may be too simplistic. For example, ghost amplitudes are often found to be lower than expected, and features indicative of acoustically induced cavitation are observed. Hence there is interest in developing approaches that allow us to solve for the ghost directly using additional measurements made in the near field. We present an approach that builds on the standard method of inverting for notional sources and that seeks to take account of nonlinear perturbations to the downgoing wavefield, including attenuation of the ghost. Perturbation of the ghost is described using a series of virtual notional sources situated in the water column between the guns and the sea surface. This is found to provide a more accurate treatment of the ghost and does not require optimization of model parameters as is often necessary in practice with the standard approach. It is also found that the inversion is more stable than an alternative parameter-free approach that solves directly for real and mirror virtual notional sources. The improved performance and stability are demonstrated with a field data example.

Introduction

Formation of a sea-surface ghost is typically associated with very different scales of pressure amplitude on the source side compared to that on the receiver side: of the order of 10 bar at the source and, for a reflection from the seabed with 1 s two-way traveltime, of the order of 10 mbar at the receiver. While a linear-acoustic representation of the wavefield is justified on the receiver side, it is questionable in the vicinity of the source (e.g., see Hampson, 2017). For arrays of guns, perhaps the most significant issue is the size of the combined ghost that is generated, which is a wave of rarefaction. When the ghost amplitude exceeds local ambient pressure, the water is put into net tension, and this will most likely lead to transient cavitation. Cavitation is the emergence and growth of microscopic vapor bubbles and is typically observed in the context of underwater explosions (Cole, 1948; Medwin and Clay, 1998). A tension pulse exceeding the strength of water will perform work during a phase of rapid expansion of the cavitation "cloud," leading to clipping of the pulse. The vapor bubbles in the cloud will then ultimately collapse as the tension falls, leading to a secondary event and emission of high frequencies (Landrø et al., 2011; Khodabandeloo and Landrø, 2018). The net effect is some loss of coherent downgoing energy in the band of interest, 2–200 Hz, which is more noticeable at high frequencies. This helps explain why the observed interference from the source ghost is often smaller than expected, even when taking into account scattering from a rough sea (Kragh and Combee, 2000; Telling et al., 2018a), and leads to estimation of reduced effective reflectivity at high frequency (Ni et al., 2012; Kyrvohuv and Campman, 2016). Other nonlinear behaviors that may take place in the near field of the source array and lead to loss of energy include formation of a spray dome at the sea surface, also called "shot effect," that arises from the doubling of particle velocity on reflection. Wave propagation velocity is dependent on amplitude, and this can lead to formation of shock fronts at high pressures and an associated energy loss due to heating. A contribution from these effects is not discounted but is relatively small compared to the onset of cavitation, which for a few milliseconds changes the state of the propagation medium. With no account made for nonlinear effects within the standard model, ringing artifacts appear in the signatures and in the seismic data, and it is necessary in practice to parameterize the ghost via the proxy of an *effective* sea-surface reflectivity, which best explains the observed data (Telling et al., 2018a). However, this is only an approximation to the downgoing wavefield, and the residual error is likely to be most significant at high frequency and contribute to acquisition-related 4D difference.

Our standard approach to signature estimation is posed as an inversion with equal numbers of source elements and hydrophones and assumes a simple ghost model with a reflection coefficient that varies with frequency according to a rough-sea scattering model (Telling et al., 2018a). The forward model for data recorded at a given hydrophone in the near field of the array is posed in the hybrid time-frequency domain (Hargreaves et al., 2015) as a linear algebraic sum of contributions from each notional source (Ziolkowski et al., 1982) and incorporates the relative motion of hydrophones and sources over time. Parkes and Hatton (1986) and Hampson (2017) propose to overcome the limitations of the simple ghost model by solving directly for the virtual notional sources that represent the ghost arrivals in addition to the real notional sources. This removes the sea-surface reflectivity parameter from the inversion but requires making

[1]Shearwater GeoServices, Tunbridge Wells, UK. E-mail: rtelling@shearwatergeo.com; sergio.grion@shearwatergeo.com.

twice as many near-field hydrophone (NFH) measurements. Telling et al. (2018b) describe a field test of this parameter-free method that gave promising results compared to the standard inversion but with a question mark over sensitivity to noise at low frequency and poorer debubble. A follow-up study into the noise sensitivity of the parameter-free method found the inversion was less stable, mainly a result of the increased (virtual) source-receiver separation and was most problematic at low frequencies due to the raised low-frequency ambient-noise profile typical of the near-surface layer of the ocean (Telling and Grion, 2019). Their proposed frequency-split hybrid of the standard and parameter-free methods provides a pragmatic way around the problem; nevertheless, an intrinsically more stable single-inversion scheme would be desirable. Here, we describe such a scheme, examine sensitivity to noise, and test results on field data acquired with two NFH channels per source element.

Method

A flexible way to represent the nonlinear interaction with the sea surface is to position secondary virtual point sources in the water column between the guns and the sea surface. The physical justification is that they represent the attenuation of the ghost due to cavitation and the subsequent signal from collapse of the cavitation cloud. The exact shape and size of the cavitation cloud is not known with precision and in practice will depend on gun configuration, sea-surface state, subarray separation, and water depth. The extent of the cloud will also be a function of time. We anticipate the origin to lie midway between subarrays, where superposition leads to the highest pressures and at a depth corresponding to where the ghost pulse magnitude exceeds ambient pressure. 2D finite-difference modeling (see Figure 1) suggests to us the initial location of the cavitation cloud is at a depth of around 3 m. We used this depth, noting that at later times the simple propagation model will no longer hold. A more complete 3D analysis of the array incorporating the subarray interaction would help refine this initial estimate.

Figure 2 illustrates the different configurations discussed here. The standard configuration solves for real notional sources and uses a simple parameterized ghost model that is optimized to minimize residual above the ghost notch (Telling et al., 2018a). With the dual NFH configuration, we can solve directly for both real and virtual notional sources without the need for prescribing reflectivity and hence call this "parameter free" (Hampson, 2017). The new scheme proposed here is similar to the standard case but with the addition of virtual sources in the water column that describe perturbation of the downgoing wavefield. Furthermore, we assume a simple deterministic ghost model with reflectivity as it is for the observed sea state and do not optimize the parameters of this model.

Our inverse problem in the frequency domain is

$$\mathbf{d} = \mathbf{G}\mathbf{m}, \tag{1}$$

where $\mathbf{d}$ is a vector corresponding to the observed pressure data at each hydrophone position, $\mathbf{m}$ is a vector corresponding to the notional sources that we wish to find by inversion, and $\mathbf{G}$ is a matrix operator that describes the propagation of acoustic energy from each source element to each hydrophone. Matrix elements are composed of a geometric scaling term $1/r$ and a phase shift based on the delay time $\exp(-i\omega r/c)$, where r is the distance from a given source element to a given hydrophone, and c is the sound speed in water. The time dependence of r due to relative motion of bubble and hydrophone is handled between inverse and forward Fourier transforms. This is implemented for the real and virtual image notional sources but not the virtual sources in the water column, which represent the perturbation to the ghost. Cavitation does not last more than a few tens of milliseconds, so its contribution to the wavefield is assumed to occur from points fixed in space. Once we have solved for the set of notional sources, we are able to calculate a far-field signature for the array at a given take-off angle by the superposition of the notional sources with appropriate phase shifts (Ziolkowski et al., 1982).

The field data used to test the signatures produced by each inversion scheme were acquired using a source with two subarrays. A schematic plan of the array is provided in Figure 3. The source elements are positioned at 7 m depth, and NFH channels are at 6 and 4 m depth and colocated in x and y for each source element. For the signature modeling, we use measured coordinates for each source element on a shot-by-shot basis and derive x and y positions from the two R-GPS receivers on each float. The z position is provided directly from the gun depth sensors.

Theoretical sensitivity to noise

Analysis of sensitivity to noise is calculated using posterior covariance. For a given system of (real and virtual) sources and hydrophones described by equation 1, the posterior covariance is:

$$\tilde{\mathbf{C}}_{\mathbf{m}} = \left(\mathbf{G}^{*}\mathbf{C}_{\mathbf{d}}^{-1}\mathbf{G} + \mathbf{C}_{\mathbf{m}}^{-1}\right)^{-1} \tag{2}$$

(Tarantola, 2005). With the prior covariance matrices assumed to be diagonal, we have, for the observed data $\mathbf{C}_{\mathrm{d}} = \sigma_d^2\mathbf{I}$, and for the model, $\mathbf{C}_{\mathrm{m}} = \sigma_m^2\mathbf{I}$, with σ_d and σ_m their respective standard deviations, $\mathbf{I}$ is the identity matrix, and the $*$ denotes complex conjugate transpose. The posterior standard deviation of the model $\tilde{\sigma}_m$ is then the square root of the diagonal of the resulting covariance matrix. We use equation 2 to calculate noise sensitivity for the various inversion schemes. For this purpose, we assume priors $\sigma_m = 1.0$ and $\sigma_d = 0.01$ at 0 Hz, reducing with frequency according to the simplified trend for observed ambient noise at an NFH, given in Figure 4.

Figure 5 shows the result of the noise sensitivity analysis for the new inversion scheme, compared against the standard and parameter-free cases. This analysis considers a first set of NFHs at 6 m depth (1 m above the guns) and a second set at 4 m. Higher sensitivity to noise is apparent at the end of the array where the relative motion of source and hydrophone leads to poorer hydrophone coverage. Figure 6 is a line plot summary at the position of black lines in Figure 5. The parameter-free inversion is clearly problematic for virtual sources at lower frequencies (less than 40 Hz), and in comparison, the new inversion is much less sensitive to noise. This is largely due to reduced separation of the notional sources and NFHs. Also, the perturbed signal is predominantly a high-frequency contribution (see Figure 7), so low-frequency sensitivity is less critical for the new method.

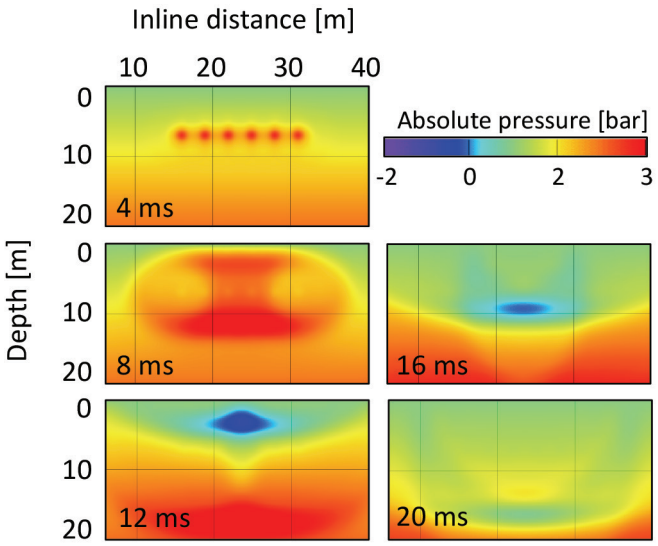

Figure 1. Snapshots from a 2D finite-difference simulation of the acoustic wavefield for a six-element array (individual source peak level 2 bar-m) linear in *x*, which is the inline direction, and firing at 7 m depth (*z*) below a perfectly reflecting flat sea surface. Ambient depth-varying hydrostatic and atmospheric pressures are superimposed. Note the transient blue region showing net tension in the water.

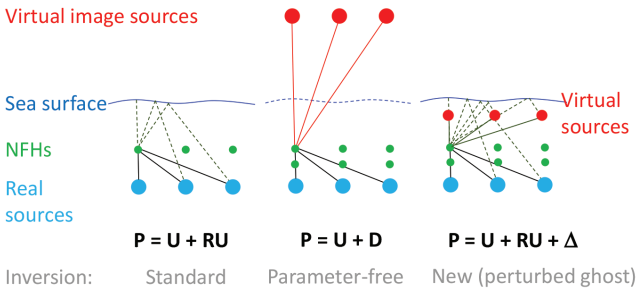

Figure 2. Schematic of the different inversion scheme geometries. The standard case is based on a single NFH per source element and where real notionals are the unknowns to be solved for. Parameter-free inversion is based on two NFH per source element solving for both real (blue) and virtual (red) sources. The new scheme is similar to the standard but with the addition of virtual sources in the water column that describe perturbation of the wavefield. Note that, kinematically, the mirror virtual source paths (red lines are parameter-free inversion) are the same as the sea-surface reflected paths (dotted lines from the real sources for standard and new inversions).

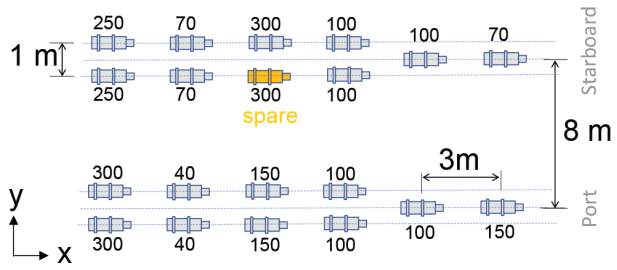

Figure 3. Source array nominal configuration comprising guns of type Teledyne Bolt Model 1500LL or 1900LLXT with capacities in the range 40–300 in³. Total volume 2740 in³. Coordinate *x* increases with distance away from vessel.

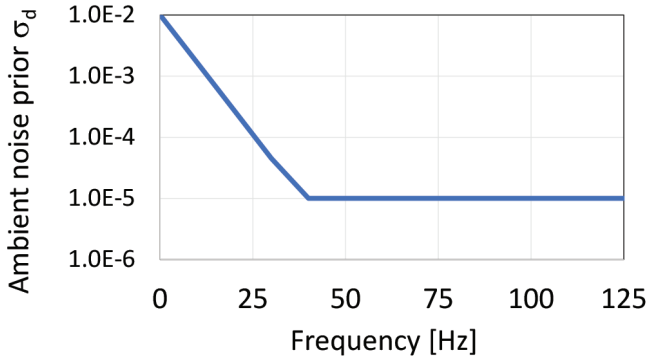

Figure 4. Prior standard deviation in the data σ_d assumed for the analysis of sensitivity to noise for the different inversion schemes. This simplified profile is taken from an NFH noise recording.

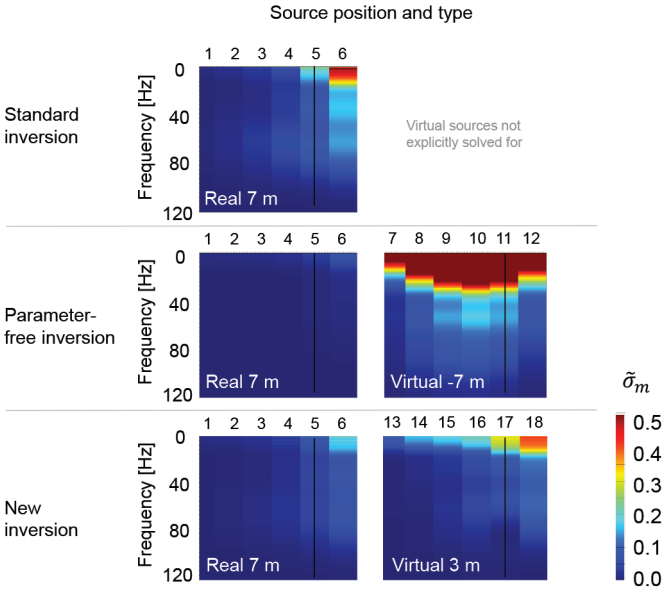

Figure 5. $\tilde{\sigma}_m$ for real notional sources 1–6 (starboard subarray, numbering increasing with *x*) at 7 m depth corresponding to each inversion, virtual sources 7–12 at image locations above the sea surface (–7 m) for the parameter-free inversion, and virtual notional sources 13–18 at 3 m below the sea surface for the new inversion. The analysis was run for the time-varying geometry for 1 s duration.

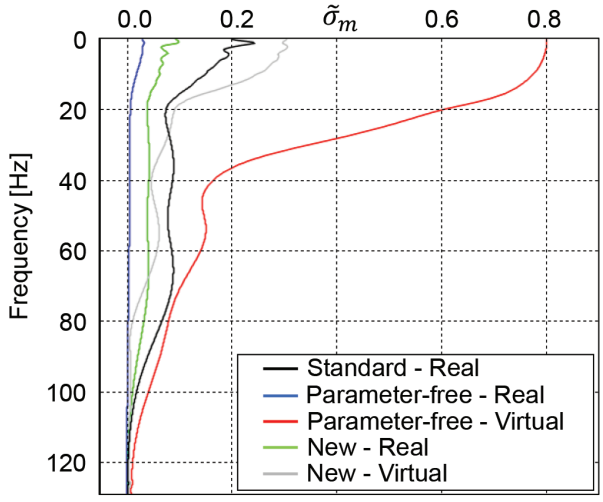

Figure 6. Summary line plots of $\tilde{\sigma}_m$ from Figure 5 (black lines).

Field data example

We apply designature to the seismic data in τ-p using directional filters derived from each set of far-field wavelets for take-off angles in the range of –30° to +70°. This process encapsulates source deghosting, debubble, and matching to a zero-phase Ormsby wavelet. Figure 7 shows an example of the estimated notional sources for one shot obtained via the new inversion scheme, including the virtual sources representing the perturbed ghost. Note the almost complete absence of bubble signature for these virtual sources, indicating that they are describing only the high-frequency perturbation of the ghost. Figure 8 shows the corresponding derived far-field signatures and a comparison against those for the standard inversion (with optimized reflectivity) and parameter-free inversion schemes. We see the initial arrivals are comparable, but Figure 9 highlights the issue with bubble oscillation for the parameter-free inversion.

Figure 10 shows the results from designature processing. For each scheme, the ghost removal appears artifact free as observed near the water bottom. However, it is clear that the parameter-free inversion mishandles bubble pulse deconvolution, which is most apparent on the direct arrival. While a hybrid of the standard and parameter-free approaches would solve this instability (Telling and Grion, 2019), the new method is attractive for its simplicity.

Conclusions

We have described an inversion approach for estimating air-gun signatures that incorporates perturbation of the source ghost due to nonlinear phenomena. The derived far fields and

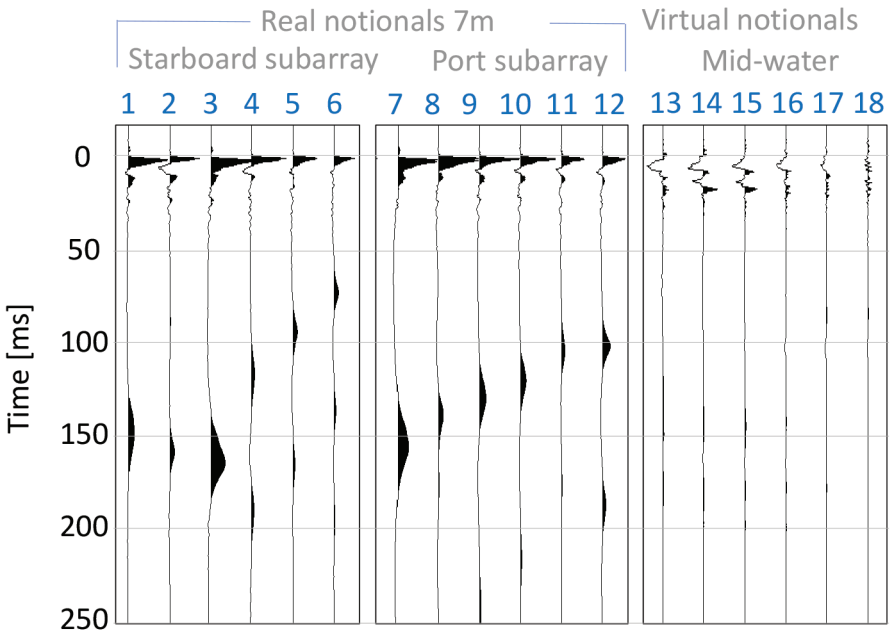

Figure 7. Example notional sources solved via the new inversion. Sources 1–12 are located at the source element coordinates. Sources 13–18 represent the ghost perturbation and are located midway between subarrays at 3 m depth. Note the character of the virtual notional traces is high frequency.

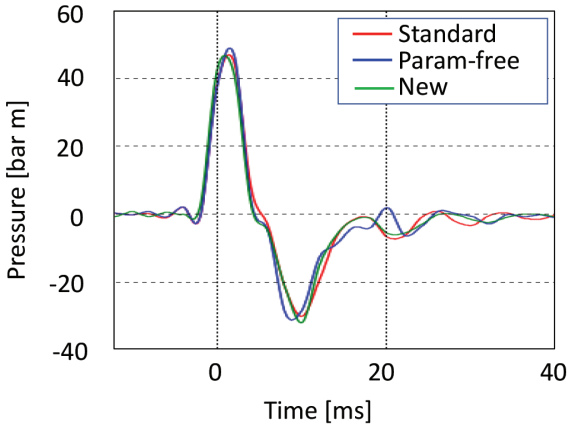

Figure 8. Vertical far-field signature showing reduced amplitude ghost and comparable initial arrivals for the three inversion schemes.

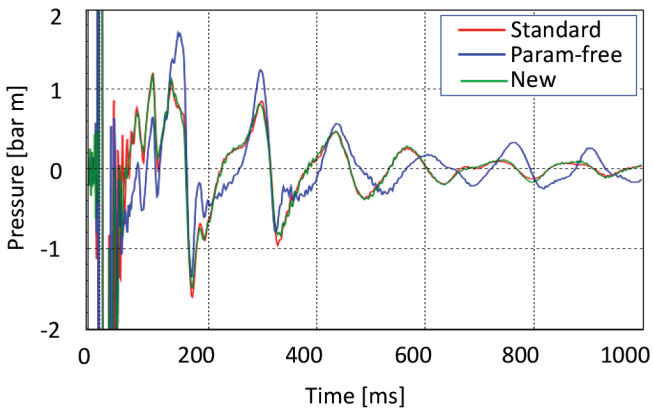

Figure 9. Vertical zoom and time-expanded plot of the vertical far-field signature from Figure 8 showing bubble oscillation for the three inversion schemes.

designature results were found to be of good quality and free of artifacts. The approach is based around solving for additional sources in the water column between subarrays and requires additional hydrophone measurements to be made in the near field of the source array. An advantage over the standard approach is that this approach better represents the physics at the source array and does not require parameter fitting or optimization of the frequency-varying reflectivity to be carried out. Further, it does not suffer the high sensitivity to noise observed for the parameter-free dual NFH method, requires fewer virtual sources, and is conceptually simpler than a hybrid of the standard and parameter-free methods. TLE

Data and materials availability

Data associated with this research are confidential and cannot be released.

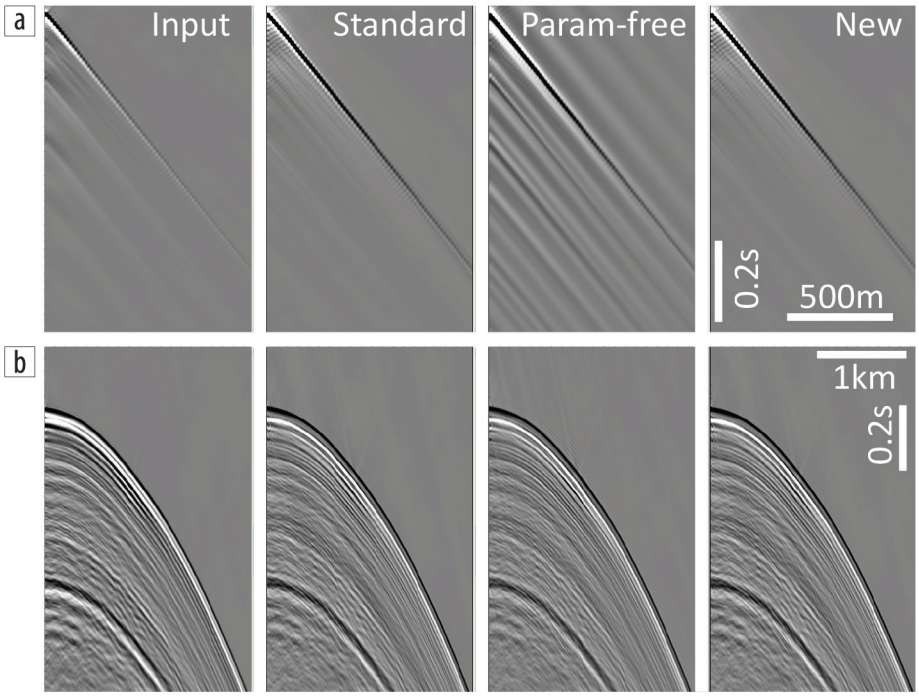

Figure 10. Example shot record before and after designature for the three inversion schemes. (a) Zoom of the direct arrival. (b) Zoom close to the seabed at 3 s two-way traveltime.

Corresponding author: rtelling@shearwatergeo.com

References

Cole, R. H., 1948, Underwater explosions: Princeton University Press.

Hampson, G., 2017, Notional ghosts: 87th Annual International Meeting, SEG, Expanded Abstracts, 111–115, https://doi.org/10.1190/segam2017-17634121.1.

Hargreaves, N., S. Grion, and R. Telling, 2015, Estimation of air-gun array signatures from near-gun measurements — Least-squares inversion, bubble motion and error analysis: 85th Annual International Meeting, SEG, Expanded Abstracts, 149–153, https://doi.org/10.1190/segam2015-5902456.1.

Khodabandeloo, B., and M. Landrø, 2018, Acoustically induced cavity cloud generated by air-gun arrays — Comparing video recordings and acoustic data to modeling: The Journal of the Acoustical Society of America, **143**, no. 6, 3383–3393, https://doi.org/10.1121/1.5040490.

Kragh, E., and L. Combee, 2000, Using a seismic reflector for resolving streamer depth and sea surface profiles: First Break, **18**, no. 11, 463–467.

Kryvohuz, M., and X. Campman, 2016, Optimization of sea surface reflection coefficient and source geometry in conventional dual source flip/flop marine seismic acquisition: 86th Annual International Meeting, SEG, Expanded Abstracts, 188–192, https://doi.org/10.1190/segam2016-13962809.1.

Landrø, M., L. Amundsen, and D. Barker, 2011, High-frequency signals from air-gun arrays. Geophysics, **76**, no. 4, Q19–Q27, https://doi.org/10.1190/1.3590215.

Medwin, H., and C. S. Clay, 1998, Fundamentals of acoustical oceanography: Academic Press, https://doi.org/10.1016/B978-0-12-487570-8.X5000-4.

Ni, Y., C. Niang, and R. Siliqi, 2012, Monitoring the stability of airgun source array signature: 82nd Annual International Meeting, SEG, Expanded Abstracts, https://doi.org/10.1190/segam2012-0875.1.

Parkes, G., and L. Hatton, 1986, The marine seismic source: Springer Netherlands, https://doi.org/10.1007/978-94-017-3385-4.

Tarantola, A., 2005, Inverse problem theory: Society of Industrial and Applied Mathematics.

Telling, R., R. Light, S. Grion, S. Denny, and G. Williams, 2018a, Signature estimation and drop-out implications for a triple source marine seismic survey: 80th Conference and Exhibition, EAGE, Extended Abstracts, https://doi.org/10.3997/2214-4609.201800742.

Telling, R., S. Grion, S. Denny, and R. G. Williams, 2018b, Marine source signature estimation with dual near-field hydrophones: 88th Annual International Meeting, SEG, Expanded Abstracts, 4070–4074, https://doi.org/10.1190/segam2018-2996061.1.

Telling, R., and S. Grion, 2019, Signature estimation using dual near-field hydrophones: Sensitivity to noise and a proposed hybrid methodology: 81st Conference and Exhibition, EAGE, Extended Abstracts, https://doi.org/10.3997/2214-4609.201901409.

Ziolkowski, A., G. Parkes, L. Hatton, and T. Haugland, 1982, The signature of an air gun array: Computation from near-field measurements including interactions: Geophysics, **47**, no. 10, 1413–1421, https://doi.org/10.1190/1.1441289.